Turkish Journal of Electrical Engineering & Computer Sciences

http://journals.tubitak.gov.tr/elektrik/

Research Article

Turk J Elec Eng & Comp Sci
(2016) 24: 3212 – 3227

doi:10.3906/elk-1408-157

A novel approach for automatic blood vessel extraction in retinal images: complex ripplet-I transform and complex valued artificial neural network

Murat CEYLAN[1,*], **Hüseyin YAŞAR**[2]
[1]Department of Electrical and Electronics Engineering, Selçuk University, Konya, Turkey
[2]Ministry of Health, Ankara, Turkey

Received: 22.08.2014 • **Accepted/Published Online:** 26.03.2015 • **Final Version:** 15.04.2016

Abstract: This study determined the features of line, curve, and ridge structures in images using complex ripplet-I and enabled extraction of blood vessel networks from retinal images through a complex valued artificial neural network using those features. Forty color fundus images in the DRIVE database and 20 color fundus images in the STARE database were used to test the success of the proposed system. In this study, a complex version of ripplet-I transform was used for the first time. By presenting the directed image for the determination of the unique geometrical properties of the vessel regions, complex ripplet-I transforms showing better performance than other types of multiresolution analysis were combined with a complex valued ANN. The results in the study were reobtained using leave-one-out cross-validation method with bagging technique in order to ensure the stability and correctness of the performance. In the DRIVE database, the highest average accuracy of the system was found to be 98.44% for complex ripplet-I transform and complex valued ANN. For the STARE database (labeled by Adam Hoover), highest average accuracy rates were obtained as 99.25% for complex ripplet-I transforms and complex valued ANN. Similarly, for the other labeled data (by Valentina Kouznetsova), highest average accuracy rates were obtained as 98.03% for complex ripplet-I transforms and complex valued ANN.

Key words: Complex ripplet-I transform, complex valued artificial neural network, blood vessel extraction, DRIVE database, STARE database

1. Introduction

The eye is one of the most important organs in the human body and provides vision and perception. Various negative environmental or genetic factors might cause dysfunction or visual impairment in this organ. A great majority of visual impairments stem from dysfunctions in structures and vessels in the retinal layer of the eye over time. Therefore, to make the right diagnosis it is first necessary to obtain and analyze retinal images of the patients. Identification of vessel distribution on retinal images, particularly through early diagnosis, has primary importance in terms of preventing visual loss due to diabetic retinopathy disease. Blood vessels in the eye should be identified for faster and more effective clinical studies. This has increased the importance of designing systems that automatically extract blood vessel structures from retinal images.

In a study carried out by Akita and Kuga [1] in 1982, the researchers tried to identify vessel distributions using connected pixels and geometric cycles. In 1996, the STARE (STructured Analysis of the REtina) database was created by Goldbaum et al. [2] in order to form a basis for further studies of some of the data. Chutatape

*Correspondence: mceylan@selcuk.edu.tr

et al. [3] suggested a method based on Gaussian and Kalman filters in order to extract vessel structures from retina images. Sinthanayothin et al. [4] achieved 83.3% sensitivity and 91.0% specificity in the identification of blood vessels. In 2000, Hoover et al. [5] obtained 65.0% sensitivity and 81.0% specificity only by using 5 RGB images. In 2004, Staal et al. [6] formed the DRIVE (Digital Retinal Images for Vessel Extraction) and STARE database and a study of these images gave 94.41% for the DRIVE database and 95.16% for the STARE database in terms of accuracy by defining a ridge-based segmentation procedure. Soraes et al. [7] used wavelet transform on the DRIVE and STARE databases in the same year. The study gave an average accuracy of 94.66% for the DRIVE database and 94.80% for the STARE database. Similarly, in 2006, Mendonça and Campilho [8] carried out a study on the extraction of blood vessels from retinal images. They obtained averaged accuracy rates of 94.52%–94.63% and 94.21%–94.79% for the DRIVE and STARE databases, respectively.

In 2007, Ricci and Perfetti [9] obtained 95.95% accuracy for the DRIVE database using line operators and support vector classification, while Martinez-Perez et al. [10] obtained 93.44% accuracy for the DRIVE database using a multiscale feature extraction method. In 2007, Feng et al. [11] determined that contourlet analysis was more successful in the representation of retina images than methods like wavelet analysis histogram equalization, local normalization, and linear unsharp masking. In the same year, Zhang et al. [12] suggested a method based on nonlinear orthogonal projection in order to extract vessel structures from retina images. The study tested on the DRIVE and STARE databases obtained an average 90.87% accuracy for the STARE database and 96.40% accuracy for the DRIVE database.

In 2008, Lam and Yan [13] developed a system respectively using the Laplacian operator and a gradient vector field. The study tested on the STARE database obtained an average 94.74% accuracy. In 2008, Kande et al. [14] conducted a study aiming to obtain vessel structures using weighted fuzzy C-means through the organization of retina images with red and green channels. That study tested on the STARE database obtained an average 93.85% accuracy.

In 2009, Akram et al. [15] conducted a study that used 2-D Gabor wavelet and sharpening filter and was tested on the STARE database and obtained 94.39% accuracy. After 2009 multiresolution analyses in blood vessel extraction from retinal images became widely used.

In 2010 Xu and Luo [16] used wavelet and curvelet transforms to extract features using the DRIVE database. They first filtered the images and then did the classification using a SVM (support vector machine). The study gave 93.2% accuracy. In the same year, Peng et al. [17] conducted a vessel segmentation study from retina images using radial projection and aggregate gradient. The study conducted on the STARE database obtained 94.22% accuracy. Moghimirad et al. [18] conducted a segmentation study based on 2D medialess function on the DRIVE and STARE databases and obtained an average 97.56% accuracy for the STARE database and 96.59% accuracy for the DRIVE database. Another segmentation study using radial projection and supervised classification was conducted by Peng et al. [19] and tested on the STARE database. The study obtained an average 94.92% accuracy. Another study by Akram and Khanum [20] that was based on wavelet transform and that used threshold probing and adaptive thresholding methods was conducted on the DRIVE and STARE databases. The study acquired an average 94.69% accuracy for the DRIVE database and 95.02% accuracy for the STARE database.

In 2011 Marin et al. [21] used gray-level and moment-invariant feature extraction methods and obtained an average accuracy of 94.52% for the DRIVE database and 95.26% accuracy for the STARE database. In the same year Miri and Mahloojifar [22] obtained 94.58% accuracy for the DRIVE database using curvelet transform.

In the same year, Fraz et al. [23] made segmentation using line strength and multiscale Gabor and morphological features. The study was tested on the DRIVE and STARE databases and obtained an average 94.76% accuracy for the DRIVE database and 95.79% accuracy for the STARE database. Another study conducted by Onkaew et al. [24] through gradient orientation analysis method obtained an average 93.58% accuracy for the DRIVE database and 94.23% for the STARE database. Fraz et al. [25] conducted a segmentation study based on morphological curvature and adapted hysteresis thresholding. The study was tested on the DRIVE and STARE databases and obtained an average 94.19% accuracy for the DRIVE database and 94.34% accuracy for the STARE database. The study conducted by Xiang et al. [26] was tested on the DRIVE and STARE databases and used combining radial symmetry transform and iterated graph cuts methods, and it obtained an average 94.45% accuracy for the DRIVE database and 95.03% accuracy for the STARE database.

In 2012, Kharghanian and Ahmadyfard [27] applied Gabor wavelet transform and line operator procedures on DRIVE database images. As a result, depending on the feature vectors, the average accuracy ranged from 94.28% to 94.94%. Devi et al. [28] and Kalaivani et al. [29] used curvelet transform to identify blood vessels from retinal images in the same year. Shahbeig [30] also used curvelet transform and obtained an average accuracy of 96.15%. In another study carried out by Shajahan and Roy [31], curvelet transform and a segmentation algorithm were used and 97.44% accuracy was obtained. Yin et al. [32] tried to obtain the vessel structure from retina images through an intensity profile with the Bayesian method. The study was tested on the STARE database and acquired an average 92.90% accuracy. In the same year, in their segmentation study, Oliveira et al. [33] primarily conducted preprocessing with combined matched filter, Frangi filter, and Gabor wavelet filter. They obtained results in two ways using oriented and region-scalable fitting energy (ORSF) and fuzzy C-means (FCM). The study was tested on the DRIVE and STARE databases and obtained an average 95.66% for the DRIVE database and 95.92% accuracy for the STARE database in the ORSF method and 95.80% accuracy for the DRIVE database and 95.82% accuracy for the STARE database in the FCM method. Again, another study conducted by Oliveira et al. [34] in the same year used the average of synthetic exact filters and Hessian matrix method and obtained an average 96.07% accuracy for the DRIVE database and 96.13% accuracy for the STARE database. Johnson et al. [35] conducted a study using curvelet and contourlet analysis on the DRIVE database in 2012 and obtained 98.4% accuracy for the curvelet-based model and 98.31% accuracy for the contourlet-based model. Silvia and Poovizhi [36] realized a segmentation application using ripplet-I and morphological gradient methods for the DRIVE database. In this study, they did not give any numerical results such as accuracy, sensitivity, or specificity values.

In 2013, Shanmugam and Banu [37] conducted segmentation based on the extreme learning machine method and tested it on the DRIVE and STARE databases. They obtained results using ten images for each database and acquired an average 97.25% accuracy for the DRIVE database and 98.62% accuracy for the STARE database. In the same year, Fraz et al. [38] conducted a segmentation study using linear discriminant classifier and tested their study on the DRIVE, STARE, and MESSIDOR databases. They obtained an average 94.52% accuracy for the DRIVE database, 95.01% accuracy for the STARE database, and 96.21% accuracy for the MESSIDOR database. Ocbagabir et al. [39] developed an automatic segmentation algorithm using the star networked pixel tracking method and 95.83% accuracy for the DRIVE database was obtained. Asad et al. [40] used ant colony optimization algorithm for 20 images on the STARE database. Accuracy rate was calculated as 91.39% according to results of their study. Another study about the DRIVE database was done by Sheet et al. [41]. They used transfer learning of tissue-specific photon interaction statistical physics and obtained an

average accuracy of 97.66%. Ceylan and Yaşar [42] proposed complex wavelet transform and a complex valued artificial neural network for retinal image segmentation. To test the methods, the DRIVE database was used and the accuracy value was calculated as 98.56%.

In the present study, we used complex ripplet-I transform and complex valued artificial neural networks for the extraction of blood vessels from retinal images. The study used no size reducing or morphological image processing technique except for complex ripplet-I analysis. A total of 60 colored fundus images (40 images from the DRIVE database and 20 images from STARE) were used in order to test the performance of the proposed system. Complex ripplet-I transforms were applied on these images and feature matrices were obtained. Using complex valued artificial neural networks, the images were recreated from feature matrices and a thresholding procedure was applied. Error between the obtained images and target images was calculated. For the network generalization, the leave-one-out cross-validation method was used. Thus, all images were used to evaluate the proposed method.

2. Methods

Curvelet analysis was introduced by Candes and Donoho [43] in 1999. In the following years, Donoho et al. [44] developed digital transform versions. Curvelet transform has created a very prevalent effect. On the other hand, the first proposed version included too much unused data. This increased the processing load and decreased the speed. In order to remove this negative situation studies related to second-generation curvelet transform definition were performed by Candes et al. [45,46]. In 2007 fast discrete curvelet transform, which depended on these studies, was proposed again by Candes et al. [47]. Together with this study, complex curvelet coefficients were also produced and this led to the definition of the complex version of the transform. In the study performed by Neelaman et al. in 2008, [48] the complex version of the transform was used. In 2010, He et al. [49] used the complex version of the transform again and performed image restoration.

In 2010, Xu et al. [50] described the ripplet-I transform, which is a higher dimensional generalization of the curvelet transform (by adding support (c) and degree (d) parameters), designed to represent images or two-dimensional signals at different scales and different directions. Together with this study, the complex version of ripplet-I transform, the real version of which had started to be used earlier, was used for the first time.

2.1. Complex ripplet-I transform

Ripplet-I transform generalizes curvelet transform by adding two parameters, support (c) and degree (d). These new parameters, c and d, provide ripplet-I with anisotropic capability of representing 2D singularities along arbitrarily shaped curves [50]. The ripplet function can be generated following the same strategy in Eq. (1).

$$\rho_{a\,\vec{b}\,\theta}(\vec{x}) = \rho_{a\,\vec{0}\,0}\left(R_\theta\left(\vec{x} - \vec{b}\right)\right) \tag{1}$$

Here, $\rho_{a\,\vec{0}\,0}(\vec{x})$ is the ripplet element function and R_θ (Eq. (2)) is the rotation matrix.

$$R_\theta = \begin{pmatrix} Cos\theta & Sin\theta \\ -Sin\theta & Cos\theta \end{pmatrix} \tag{2}$$

The element ripplet function $\rho_{a\vec{0}0}$ with scale parameter a is defined in the frequency domain in polar coordinates [50]. Eq. (3) expresses curvelet transform for values $c = 1,\ d = 2$.

$$\hat{\rho}_\theta(r,\omega) = \frac{1}{\sqrt{c}} a^{\frac{1+d}{2d}} W(a.r)\, V\left(\frac{a^{\frac{1}{d}}}{c.a}.\omega\right) \tag{3}$$

The discrete transform takes as input data defined on a Cartesian grid and outputs a collection of coefficients. For the scale parameter a, we sample at dyadic intervals. The position parameter b and rotation parameter θ are sampled at equal-spaced intervals. a, $\vec{b}$, and θ are substituted with discrete parameters a_j, $\vec{b}_k$, and θ_l, which satisfy that $a_j = 2^{-j}$, $\vec{b}_k = \left[c.2^{-j}.k_1, 2^{-j/d}.k_2\right]^T$, and $\theta_l = \frac{2\pi}{c}.2^{-|j(1-1/d)|}.l$, where $\vec{k} = [k_1,k_2]^T$, $(.)^T$ denotes the transpose of a vector and $j, k_1, k_2, l \in Z$. The frequency response of ripplet function is given as ($d = n\ /\ m$ and $n,\ m \neq 0 \in$ Z) [50].

$$\hat{\rho}_j(r,\omega) = \frac{1}{\sqrt{c}} a^{\frac{m+n}{2n}} W\left(2^{-j}.r\right) V\left(\frac{2^{-j\left|\frac{m-n}{n}\right|}}{c}.\omega - l\right) \tag{4}$$

Here, W and V satisfy the following conditions:

$$\sum_{j=0}^{\infty} \left|W(2^{-j}.r)\right|^2 = 1 \text{ and } \sum_{l=-\infty}^{+\infty} \left|V(\frac{2^{-j|1-1/d|}}{c}.\omega - l)\right|^2 = 1 \tag{5}$$

The goal here is to find a digital implementation of the discrete ripplet-I transform, whose coefficients are now given by

$$r_{j,k,l} := \left\langle f.\rho^D_{j,k,l} \right\rangle = \int_{R^2} \hat{f}(v)\tilde{\rho}^D_j(S^{-1}_{\theta_j}v) e^{iS^{-T}_{\theta_j} m.v} dv \tag{6}$$

where S_θ is the shear matrix (Eq. (7)) and $m \approx \left[c.2^{-j}.k_1, 2^{-j/d}.k_2\right]$.

$$S_\theta := \begin{pmatrix} 1 & 0 \\ -Tan\theta & 1 \end{pmatrix} \tag{7}$$

The operations after this stage are conducted as defined earlier by fast discrete curvelet transform [47]. $\tilde{U}_{j,l}[n_1,n_2]$ reindexing the samples array by wrapping around a $\approx c.2^j \times 2^{j/d}$ (width $\approx c \times$ (length)^d) rectangle centered at the origin. The ripplet-I via wrapping is described below with the basic steps.

Step 1: Compute 2D FFT coefficients to obtain Fourier samples $\hat{f}[n_1,n_2]$.

Step 2: Interpolation for each scale and angle pair (j,l), $\tilde{U}_{j,l}[n_1,n_2]\hat{f}[n_1,n_2]$.

Step 3: Wrap result of Step 2 around the origin and obtain $\tilde{f}[n_1,n_2] = W(\tilde{U}_{j,l}\tilde{f})[n_1,n_2]$ where the ranges n_1 and n_2 are $0 \leq n_1 \leq L_{1,j}$ and $0 \leq n_2 \leq L_{2,j}$, respectively.

Step 4: Implement the inverse 2D FFT for each $\tilde{f}_{j,l}$ to obtain the discrete coefficients.

The discrete ripplet-I transform coefficients are complex valued, but a real valued discrete ripplet-I transform with the same redundancy factor can be easily obtained by properly combining coefficients at orientations θ_l and $\theta_l + \pi$. Coefficients of ripplet-I can be expressed as follows. $RP - I_R$ and $RP - I_I$ are real and imaginary coefficients, respectively.

$$RP - I = RP - I_R + j.RP - I_I \tag{8}$$

In this study, the MATLAB codes located in *curvelab* [51] were used by adapting to ripplet-I transform for values $c = 1$, $d = 3$.

2.2. Complex valued artificial neural networks

Artificial neural networks (ANNs) can be described as a computer science interested in adaptive information processing developed for the events whose programming is difficult or impossible. Although there are different types of ANNs, the most widely used type is backpropagation ANN. Backpropagation ANN is an artificial intelligence algorithm consisting of an input layer, hidden layer, and output layer. The input layer contains data that are presented to the ANN (one- or two-dimensional). The input layer and hidden layer, and the hidden layer and output layer, are associated with process elements called weight. In parallel with the counseling learning principle, the ANN is given both inputs and targets. Weighted sums of each layer are passed through a nonlinear function (called an activation function or transfer function). Although various activation functions (step, linear, logarithmic sigmoid, tangent sigmoid, etc.) of each layer can be considered, the logarithmic sigmoid activation function was used in this study. The ANN produces outputs compatible with the given inputs and calculates an error value based on the difference between the target and produced output. When the error value is outside the tolerance margin, the weight coefficients are recalculated in a backward direction. The procedure called training is ended when the ANN, which produces new outputs in line with the new weight coefficients, reaches the desired error value. Using the obtained weight coefficients from this iterative training process, the ANN test procedure is performed through the data that have not been introduced to the network [52].

In a complex backpropagation model all inputs, weights, threshold, and output patterns are complex numbers [52]. Figure 1 shows a complex valued ANN model. The instance that is complex in nature presented to the network is the activation level of the input. The output A_k of neuron k is defined as:

$$A_k = F(\sum W_{k,i}.x_i + \theta_k) \tag{9}$$

$$W_{k,i} = Re\,[W_{k,i}] + iIm\,[W_{k,i}] \tag{10}$$

$W_{k,i}$ (Eq. (10)) is the complex weight from an input. x_i is the unit and θ_k is the complex valued threshold. Although various output functions of each neuron can be considered, the output function used in this study is defined by the following equation:

$$F_C(z) = F_R(x) + i.F_R(y) \tag{11}$$

where $F_R(a) = \frac{1}{1+e^{-a}}$ and is called the sigmoid function.

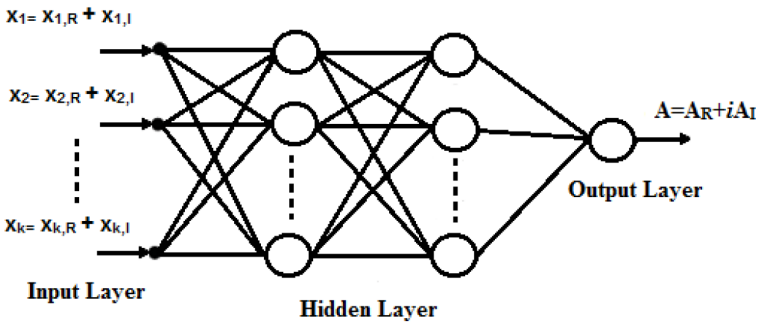

Figure 1. A model of the complex valued ANN.

In this study, feature matrices obtained by complex ripplet-I transform contain complex valued components in addition to real valued components. At this stage, real components of feature matrices can be evaluated with a conventional ANN. When using the existing method for real features, we must apply the method individually to their real and imaginary parts. On the other hand, the complex valued ANN allows us to directly process features. Moreover, complex valued components will not be obtained when the inverse of the transform is applied. To achieve better accuracy, the complex valued ANN is used.

2.3. Used data

This study used 40 colorful fundus images (and segmented targets) from the DRIVE database and 20 colorful fundus images from the STARE database [5,6]. Target images in the present study were used in order to compare the DRIVE database with the literature. These images are in 584 $\times$ 565 size and JPEG format. DRIVE database images are arranged in 512 $\times$ 512 size. A target image labeled by two different experts was used in order to determine the labeling mistakes and test the reliability of results for the STARE database. The images in the STARE database were in PPM format and 605 $\times$ 700 in size. STARE database images are arranged in 576 $\times$ 576 size.

3. Experiments and results

3.1. Experiments

In this study, blood vessels in retinal images were extracted using complex ripplet-I and a complex valued ANN. A total of 60 images from the DRIVE and STARE databases and 60 target images formed by the extraction of blood vessels in these images were used to evaluate the proposed method. To determine the features of line, curve, and ridge structures in images, complex ripplet-I transforms with three scales were used. All coefficients in the subbands are presented to the ANN because small coefficient values and big coefficient values indicate different structures in the retinal images such as noise, background, and vessels, respectively.

Complex ripplet-I transform was applied to retina images in the first part of the study. In the DRIVE database, 21 $\times$ 21 sized feature (coefficient) matrices were used for scale = 6, 43 $\times$ 43 sized feature (coefficient) matrices were used for scale = 5, and 85 $\times$ 85 sized matrices were used for scale = 4. In the STARE database, 25 $\times$ 25 sized feature (coefficient) matrices were used for scale = 6, 49 $\times$ 49 sized feature (coefficient) matrices were used for scale = 5, and 97 $\times$ 97 sized matrices were used for scale = 4. The difference between the sizes of feature matrices results from the difference between the sizes of images used in both databases and therefore causes the filters in the transformation structure to produce coefficients of different lengths. Coefficients contained by these matrices represent the lines, transit points, peak points, etc. formed by blood vessels in the retinal image. These obtained feature matrices were entered into the complex valued ANN as input. Similarly, the transforms were applied to the target images and the coefficients given to the complex valued ANN as input were desired to be accurately estimated in the output. The coefficients obtained from the output of the complex valued ANN were resized by taking inverse transforms. After that, binary thresholding (binary morphological operation) was applied and the difference between the target image and output (error) was calculated. At this stage, the real dimension reobtained by complex ripplet-I transform and complex valued ANN was used in the operation. A block diagram of the proposed structure is presented in Figure 2.

3.2. Evaluation of results

The proportion of the number of correct classified pixels (CCP) to total pixels (ToP) in the image was calculated in the evaluation of the study results (Eq. (12)).

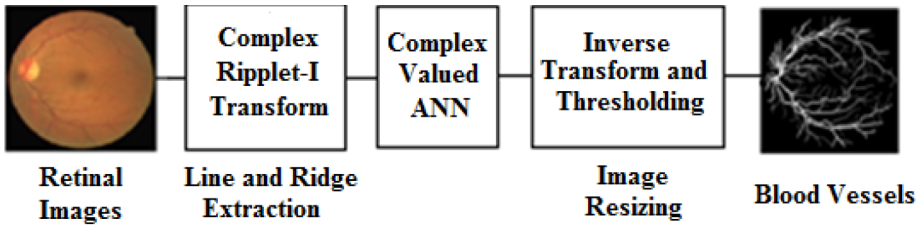

Figure 2. Proposed method for blood vessel extraction.

$$\text{Accuracy } (\%) = (CCP/ToP) \times 100 \tag{12}$$

In order to determine the success of the separation of the background from the vessel regions of the proposed system, statistical measures such as sensitivity and specificity are used.

1) True positive (TP): The ANN identifies an input as a vessel labeled by the expert clinicians.

2) True negative (TN): The ANN identifies an input as a background that was labeled as background by the expert clinicians.

3) False positive (FP): The detection of a vessel that was labeled as background by the expert.

4) False negative (FN): The detection of a background that was labeled as a vessel patient by the expert.

The performance of the classifier is also assessed in terms of sensitivity as follows:

$$SEN = TP/(TP + FN) \tag{13}$$

3.3. Results

A backpropagation ANN with one hidden layer, which uses the Levenberg–Marquardt learning algorithm, was preferred in this study. A logarithmic sigmoid function defined in the [0,1] range is used as the activation function in the ANN structure. The weights used are renewed by calculating the difference (error) between the value obtained from the ANN output and target. The appropriate iteration number for the ANN model used in this study is determined as 1000. The number of neurons in the hidden layer is found to be eight and in the learning rate is found to be 0.05, empirically. It is known that the number of hidden nodes greatly affects the performance of an ANN. Hence, tests were conducted with between 0 and 200 hidden nodes to determine the optimum number of hidden nodes. It was observed that a node number of eight requires the least training and yielded the smallest errors after the learning rate was increased in increments from 0.001 to 5.0, provided that the optimum hidden node was pegged. It was also observed that the iteration number at which the moment constant becomes 0.2 was 1000.

At the end of the training and test procedures, in the DRIVE database, the average accuracy of the system was found to be 97.85% (scale = 4), 98.43% (scale = 5), and 98.44% (scale = 6) for complex ripplet-I transform and complex valued ANN.

The leave-one-out cross-validation method was used for the generalization of the ANN. While 39 images from the database formed from a total of 40 images were used in ANN training, ANN testing was performed using the remaining image. Then the image used for the test was included in the training process and ANN testing was performed by using one of the images used in the training. By repeating the same iterative process 40 times, the reliability of the obtained results is increased via all images in the database.

The STARE database was used in order to test system performance with different background intensity, noise, and degeneration. Similarly, the same processes were applied to 20 images of STARE database. Obtained

images and target images labeled by Adam Hoover and Valentina Kouznetsova were separately compared. For the STARE database (labeled by Adam Hoover), accuracy rates were obtained as 98.40% (scale = 4), 99.15% (scale = 5), and 99.25% (scale = 6) for complex ripplet-I transform and complex valued ANN. For the other labeled data (by Valentina Kouznetsova), accuracy rates were obtained as 96.72% (scale = 4), 97.80% (scale = 5), and 98.03% (scale = 6) for complex ripplet-I transform and complex valued ANN.

Results of DRIVE and STARE images are presented in Table 2. In the table, NCCP refers to the number of correct classified pixels and NICP refers to the number of incorrect classified pixels. The proposed methods were compared using the SEN statistical method and the results are given in Table 2.

Table 1. Optimum ANN architecture.

Error goal	No. of hidden nodes	Learning rate	Momentum constant	No. of maximum iterations
1e-20	8	0.05	0.2	1000

Table 2. Results for DRIVE and STARE databases.

Data	Test			
	NCCP	NICP	Accuracy (%)	SEN
DRIVE database (scale = 4)	256,495	5649	97.85	0.794
DRIVE database (scale = 5)	258,018	4126	98.43	0.852
DRIVE database (scale = 6)	258,049	4095	98.44	0.853
STARE database labeled by A Hoover (scale = 4)	326,463	5313	98.40	0.945
STARE database labeled by V Kouznetsova (scale = 4)	320,880	10,896	96.72	0.900
STARE database labeled by A Hoover (scale = 5)	328,958	2818	99.15	0.971
STARE database labeled by V Kouznetsova (scale = 5)	324,476	7300	97.80	0.933
STARE database labeled by A Hoover (scale = 6)	329,299	2477	99.25	0.974
STARE database labeled by V Kouznetsova (scale = 6)	325,232	6544	98.03	0.940

Randomly selected images (no.1; no.8) from the DRIVE and STARE databases are given in Figure 3 (a1; b1), respectively. (a2), (a3), and (a4) in Figure 3 present ANN outputs for the DRIVE database. Similarly, (b2), (b3), and (b4) in Figure 3 present ANN outputs for the STARE database. Scale values are 4, 5, and 6 for all of the images in these figures. Target images for these databases are given in Figure 3 ((a5), (b5), and (b6)).

From the comparison of the proposed method with previous studies that used the DRIVE and STARE databases (with the same images), it was observed that it gave a higher accuracy value. The comparison is presented in Tables 3 and 4.

As can be seen in Tables 3 and 4, by combining the complex ripplet-I transform with the complex valued ANN, more successful results were obtained when compared with using only multiresolution analysis or using them with classifiers (kNN, SVM, etc.). The success of the proposed system in terms of separating vessels from the background is revealed by the success of complex ripplet-I transform in representing (separating) the image and the success of the complex valued ANN in classifying feature matrices. Most of the studies given in Tables 3 and 4 do not have information about segmentation time. This study was performed using a computer with a 2.00 GHz processor and 4 GB RAM, and segmentation time per image was 6.27 s for complex ripplet-I transform.

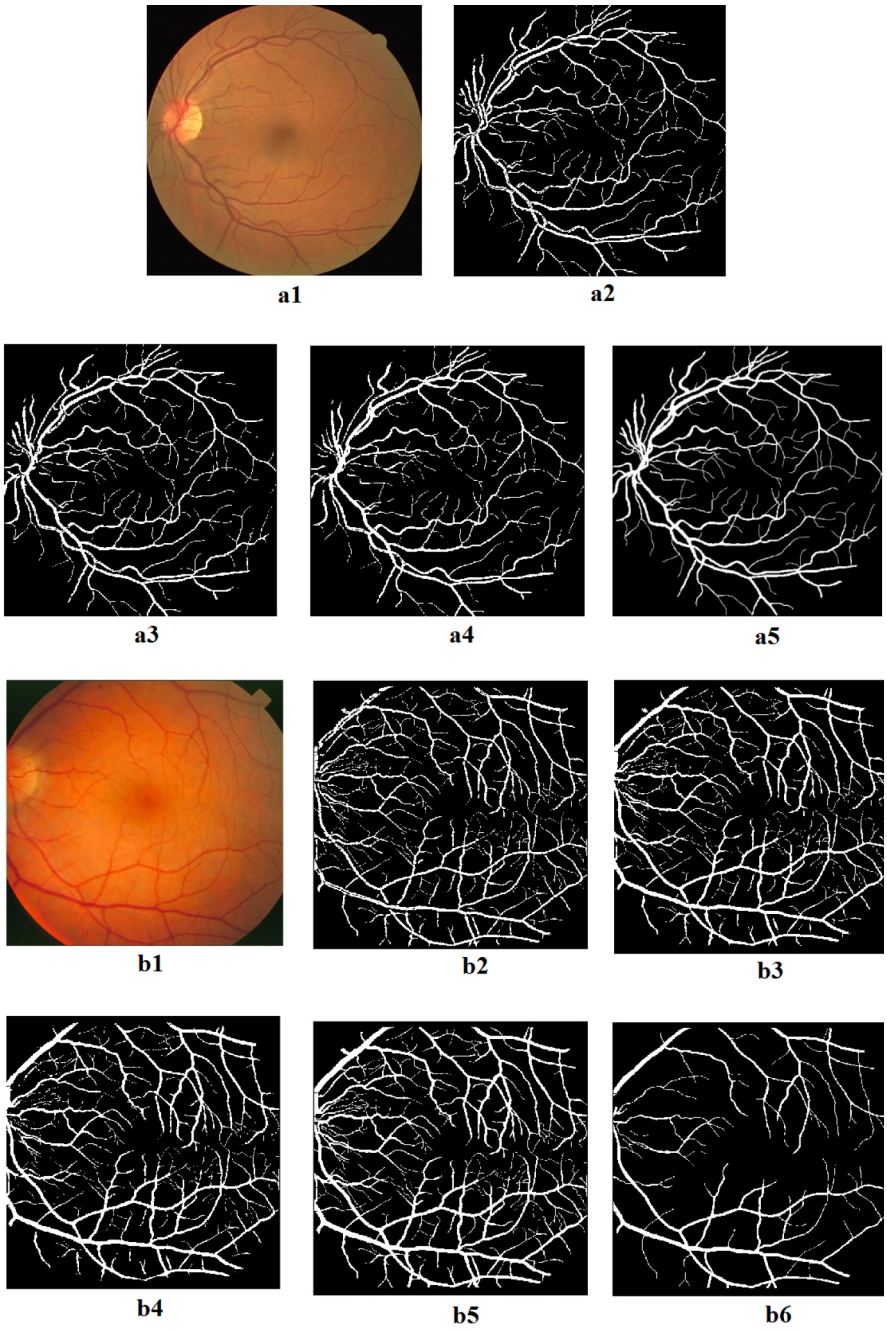

Figure 3. Resultant images for DRIVE and STARE databases (DRIVE database): a1) Original image no.1, a2) Result of complex ripplet-I transform for image no.1 (scale = 4), a3) Result of complex ripplet-I transform for image no.1 (scale = 5), a4) Result of complex ripplet-I transform for image no.1 (scale = 6), a5) Target for image no.1; (STARE database) b1) Original image no.8, b2) Result of complex ripplet-I transform for image no.8 (scale = 4), b3) Result of complex ripplet-I transform for image no.8 (scale = 5), b4) Result of complex ripplet-I transform for image no.8 (scale = 6), b5) Target for image no.8 (V Kouz.), b6) Target for image no.8 (A Hoover).

Table 3. Comparison of the proposed method and other methods in previous studies for DRIVE database.

Study	Year	Methods	Accuracy (%)
Staal et al. [6]	2004	Image ridges and kNN classifier	94.41
Soares [7]	2006	Gabor wavelet	94.66
Mendonça and Campilho [8]	2006	Combining of morphological reconstruction and centerlines detection	94.52–94.63
Ricci and Perfetti [9]	2007	Line operator and support vector machine (SVM)	95.95
Martinez-Perez et al. [10]	2007	Multiscale feature extraction	93.44
Zhang et al. [12]	2007	Nonlinear orthogonal projection	96.40
Xu and Luo [16]	2010	Curvelet transform, wavelet transform, and SVM	93.2
Moghimirad et al. [18]	2010	2D medialess function	96.59
Akram and Khanum [20]	2010	Wavelet transform, threshold probing, and adaptive thresholding	94.69
Marin et al. [21]	2011	Gray-level and moment-invariant feature extraction	94.52
Miri and Mahloojifer [22]	2011	Curvelet transform	94.58
Fraz et al. [23]	2011	Line strength, multiscale Gabor, and morphological features	94.76
Onkaew et al. [24]	2011	Gradient orientation analysis	93.58
Fraz et al. [25]	2011	Morphological curvature and adapted hysteresis thresholding	94.19
Xiang et al. [26]	2011	Combining radial symmetry transform and iterated graph cuts	94.45
Kharghanian and Ahmadyfard [27]	2012	Gabor wavelet transform and line operator	94.28–94.94
Shahbeig [30]	2012	Curvelet transform, component analysis, adaptive filter	96.15
Shajahan and Roy [31]	2012	Multistructure elements morphology	97.44
Oliveira et al. [33]	2012	Combined matched filter, Frangi filter, Gabor wavelet filter, oriented and region-scalable fitting energy	95.66
		Combined matched filter, Frangi filter, Gabor wavelet filter, fuzzy C-means	95.80
Oliveira et al. [34]	2012	Average of synthetic exact filters and Hessian matrix	96.07
Johnson et al. [35]	2012	Curvelet transform	98.4
		Contourlet transform	98.31
Silvia and Poovizhi [36]	2012	Ripplet-I and morphological gradient	-
Shanmugam and Banu [37]	2013	Extreme learning machine	97.25
Fraz et al. [38]	2013	Linear discriminant classifier	94.52
Ocbagabir et al. [39]	2013	Star networked pixel tracking	95.83
Sheet et al. [41]	2013	Transfer learning of tissue specific photon interaction statistical physics	97.66
Ceylan and Yaşar [42]	2013	Complex wavelet transform and complex valued ANN	98.56
Our study	2014	Complex Ripplet-I transform and complex valued ANN (scale = 4) Complex Ripplet-I transform and complex valued ANN (scale = 5) Complex Ripplet-I transform and complex valued ANN (scale = 6)	97.85 98.43 98.44

Table 4. Comparison of the proposed method and other methods in previous studies for STARE database.

Study	Year	Methods	Accuracy (%)
Staal et al. [6]	2004	Image ridges and kNN classifier	95.16
Soares [7]	2006	Gabor wavelet	94.80
Mendonça and Campilho [8]	2006	Combining of morphological reconstruction and centerlines detection	94.21–94.79
Zhang et al. [12]	2007	Nonlinear orthogonal projection	90.87
Lam and Yan [13]	2008	Laplacian operator and gradient vector field	94.74
Kande et al. [14]	2008	Red and green channels and weighted fuzzy C-means	93.85
Akram et al. [15]	2009	2-D Gabor wavelet and sharpening filter	94.39
Peng et al. [17]	2010	Radial projection and aggregate gradient	94.22
Moghimirad et al. [18]	2010	2D medialess function	97.56
Peng et al. [19]	2010	Radial projection and supervised classification	94.92
Akram and Khanum [20]	2010	Wavelet transform, threshold probing, and adaptive thresholding	95.02
Marin et al. [21]	2011	Gray-level and moment-invariants feature extraction	95.26
Fraz et al. [23]	2011	Line strength, multiscale Gabor, and morphological features	95.79
Onkaew et al. [24]	2011	Gradient orientation analysis	94.23
Fraz et al. [25]	2011	Morphological curvature and adapted hysteresis thresholding	94.34
Xiang et al. [26]	2011	Combining radial symmetry transform and iterated graph cuts	95.03
Yin et al. [32]	2012	Bayesian method	92.90
Oliveira et al. [33]	2012	Combined matched filter, Frangi filter, Gabor wavelet filter, oriented and region-scalable fitting energy	95.92
		Combined matched filter, Frangi filter, Gabor wavelet filter, fuzzy C-means	95.82
Oliveira et al. [34]	2012	Average of synthetic exact filters and Hessian matrix	96.13
Shanmugam and Banu [37]	2013	Extreme learning machine	98.62
Fraz et al. [38]	2013	Linear discriminant classifier	95.01
Asad et al. [40]	2013	Ant colony system	91.39
Our study (labeled by A Hoover)	2014	Complex Ripplet-I transform and complex valued ANN (scale = 4) Complex Ripplet-I transform and complex valued ANN (scale = 5) Complex Ripplet-I transform and complex valued ANN (scale = 6)	98.40 99.15 99.25
Our study (labeled by V Kouznetsova)	2014	Complex Ripplet-I transform and complex valued ANN (scale = 4) Complex Ripplet-I transform and complex valued ANN (scale = 5) Complex Ripplet-I transform and complex valued ANN (scale = 6)	96.72 97.80 98.03

4. Discussion and conclusions

This study proposed the use of complex valued ANN architecture with complex ripplet-I transform for the procedure of the extraction of blood vessels in retinal images. At the end of the study, the obtained results were much better than those in some studies [16,22,29,30,35] where curvelet transform was used. One of the basic reasons for the success of this study is that ripplet-I transform, which is the generalized version of curvelet transform, was used in the study. It is known from the previously made study [42] that the usage of the complex versions of the transforms has a positive impact on the study results. In this study, the usage of a complex version of ripplet-I transform has increased the success of the study. On the other hand, usage of an ANN instead of SVM is another factor that has increased the success of the study. The SVM tries to obtain thin vessel structures by iterative estimations from the images, obtaining large vessel structures. However, the ANN considers the image as a whole instead of making the distinction of thin vessel structures. This makes it easy to associate vessels with each other. On the other hand, the nature of SVMs, which are more convenient in terms of working with small data sets and performing classification of neural classifiers using easier control, and which have lower computation requirements, reveals the reason why the ANN obtains more successful results compared with similar studies.

The proposed system being tested by different background intensities and noises (STARE database) as well as the DRIVE database has increased the reliability of the study results. Together with the usage of target displays labeled by two different people for the STARE database, the effect of label difference on the general success of the system was observed. The proposed system has produced very good results for even much more complex labeling including small vein structures. Besides, as the scale value increased for ripplet-I transform, namely as the size of the property matrix where operation is made decreased, it was observed that the system success increased.

Feature matrices were excluded from the suggested structure through multiple resolution analysis since the ANN produces faster solutions with higher accuracy. Passing image matrices directly to the ANN without any preprocessing increases the number of operations and makes the convergence of the ANN to the target difficult.

Together with this study, the complex version of ripplet-I transform, the real version of which started to be used earlier, was used for the first time. As a result of this study, satisfactory numerical results were obtained using complex ripplet-I transform for the extraction of blood vessels in retinal images for the first time. Obtained results of the complex ripplet-I transform are better than those of curvelet transform. This situation will be experienced in the field of multiresolution analysis of recent development that has proven that it is important for medical image processing.

Even though other studies used different transforms, the inclusion of an ANN in the proposed structure increased accuracy. The presence of the ANN enabled an automated solution and developed a different perspective through creating a basis for different artificial intelligence approaches. Different accuracy levels can be obtained through changing the model, structure, parameters, etc. of the ANN, which is important for creating a new solution-targeted approach. The development of semi/fully automatic systems in the segmentation of medical images in particular demonstrates the fact that ANNs and similar structures are an important part of the solution.

References

[1] Akita K, Kuga H. A computer method of understanding ocular fundus images. Pattern Recogn 1982; 15: 431-443.

[2] Goldbaum M, Moezzi S, Taylor A, Chatterjee S, Boyd J, Hunter E, Jain R. Automated diagnosis and image understanding with object extraction, object classification, and inferencing in retinal images. In: IEEE International Conference Image Processing; 16–19 September 1996; Lausanne, Switzerland. New York, NY, USA: IEEE. pp. 695-698.

[3] Chutatape O, Zheng L, Krishnan SM. Retinal blood vessel detection and tracking by matched Gaussian and Kalman filters. In: IEEE International Conference Engineering in Medicine and Biology Society; 29 October–1 November 1998; Hong Kong. New York, NY, USA: IEEE. pp. 3144-3149.

[4] Sinthanayothin C, Boyce JF, Cook HL, Williamson TH. Automatic localisation of the optic disk, fovea, and retinal blood vessels from digital colour fundus images. Brit J Ophthalmol 1999; 83: 902-910.

[5] Hoover AD, Kouznetsova V, Goldbaum M. Locating blood vessels in retinal images by piece-wise threshold probing of a matched filter response. IEEE T Med Imaging 2000; 19: 203-210.

[6] Staal J, Abramoff MD, Niemeijer M, Viergever MA, Ginneken B. Ridge based vessel segmentation in color images of the retina. IEEE T Med Imaging 2004; 23: 501-509.

[7] Soares JVB, Leandro JJG, Cesar RM, Jelinek HF, Cree MJ. Retinal vessel segmentation using the 2-D Gabor wavelet and supervised classification. IEEE T Med Imaging 2006; 25: 1214-1222.

[8] Mendonça AM, Campilho A. Segmentation of retinal blood vessels by combining the detection of centerlines and morphological reconstruction. IEEE T Med Imaging 2006; 25: 1200-1213.

[9] Ricci E, Perfetti R. Retinal blood vessel segmentation using line operators and support vector classification. IEEE T Med Imaging 2007; 26: 1357-1365.

[10] Martinez-Perez ME, Hughes AD, Thom SA, Bharath AA, Parker KH. Segmentation of blood vessels from red-free and fluorescein retinal images. Med Image Anal 2007; 11: 47-61.

[11] Feng P, Pan Y, Wei B, Jin W, Mi D. Enhancing retinal image by the contourlet transform. Pattern Recogn Lett 2007; 28: 516-522.

[12] Zhang Y, Hsu W, Lee ML. Segmentation of retinal vessels using nonlinear projections. In: IEEE International Conference on Image Processing; 16 September–19 October 2007; San Antonio, TX, USA. New York, NY, USA: IEEE. pp. 541-544.

[13] Lam BSY, Yan H. A novel vessel segmentation algorithm for pathological retina images based on the divergence of vector fields. IEEE T Med Imaging 2008; 27: 237-246.

[14] Kande GB, Savithri TS, Subbaiah PV. Retinal vessel segmentation using spatially weighted fuzzy c-means clustering and histogram matching. In: IEEE India Conference; 11–13 December 2008; Kanpur, India. New York, NY, USA: IEEE. pp. 1-6.

[15] Akram MU, Atzaz A, Aneeque SF, Khan SA. Blood vessel enhancement and segmentation using wavelet transform. In: IEEE International Conference on Digital Image Processing; 7–9 March 2009; Bangkok, Thailand. New York, NY, USA: IEEE. pp. 34-38.

[16] Xu L, Luo S. A novel method for blood vessel detection from retinal images. Biomed Eng Online 2010; 9: 1-14.

[17] Peng Q, Peng G, Xu D, You X, Pang B. A fast approach to retinal vessel segmentation. In: Chinese Conference on Pattern Recognition; 21–23 October 2010; Chongqing, China. New York, NY, USA: IEEE. pp. 1-5.

[18] Moghimirad E, Rezatofighi SH, Soltanian-Zadeh H. Multi-scale approach for retinal vessel segmentation using medialness function. In: IEEE International Symposium on Biomedical Imaging: From Nano to Macro; 14–17 April 2010; Rotterdam, the Netherlands. New York, NY, USA: IEEE. pp. 29-32.

[19] Peng Q, You X, Zhou L, Cheung Y. Retinal blood vessels segmentation using the radial projection and supervised classification. In: International Conference on Pattern Recognition; 23–26 August 2010; İstanbul, Turkey. New York, NY, USA: IEEE. pp. 1489-1492.

[20] Akram MU, Khanum A. Retinal images: blood vessel segmentation by threshold probing. In: IEEE Symposium on Industrial Electronics & Applications; 3–5 October 2010; Penang, Malaysia. New York, NY, USA: IEEE. pp. 493-497.

[21] Marin D, Aquino A, Gegundez-Arias ME, Bravo JM. A new supervised method for blood vessel segmentation in retinal images by using gray-level and moment invariants-based features. IEEE T Med Imaging 2011; 30: 146-158.

[22] Miri MS, Mahloojifar A. Retinal image analysis using curvelet transform and multistructure elements morphology by reconstruction. IEEE T Bio-Med Eng 2011; 58: 1183-1191.

[23] Fraz MM, Remagnino P, Hoppe A, Velastin S, Uyyanonvara B, Barman SA. A supervised method for retinal blood vessel segmentation using line strength, multiscale Gabor and morphological features. In: IEEE International Conference on Signal and Image Processing Applications; 16–18 November 2011; Kuala Lumpur, Malaysia. New York, NY, USA: IEEE. pp. 410-415.

[24] Onkaew D, Turior R, Uyyanonvara B, Kondo T. Automatic extraction of retinal vessels based on gradient orientation analysis. In: International Joint Conference on Computer Science and Software Engineering; 11–13 May 2011; Nakhon Pathom, Thailand. New York, NY, USA: IEEE. pp. 102-107.

[25] Fraz MM, Basit A, Remagnino P, Hoppe A, Barma SA. Retinal vasculature segmentation by morphological curvature, reconstruction and adapted hysteresis thresholding. In: International Conference on Emerging Technologies; 5–6 September 2011; Islamabad, Pakistan. New York, NY, USA: IEEE. pp. 1-6.

[26] Xiang D, Tian J, Deng K, Zhang X, Yang F, Wan X. Retinal vessel extraction by combining radial symmetry transform and iterated graph cuts. In: International Conference of the IEEE Engineering in Medicine and Biology Society; 30 August–3 September 2011; Boston, MA, USA. New York, NY, USA: IEEE. pp. 3950-3953.

[27] Kharghanian R, Ahmadyfard A. Retinal blood vessel segmentation using Gabor wavelet and line operator. International Journal of Machine Learning and Computing 2012; 2: 593-597.

[28] Devi KK, Anto A, Peter KJ. Curvelet transform and multi structure elements morphology by reconstruction based retinal image analysis. International Journal of Soft Computing and Engineering 2012; 2: 548-553.

[29] Kalaivani M, Jeyalakshmi MS, Aparna V. Extraction of retinal blood vessels using Curvelet transform and Kirsch's templates. International Journal of Emerging Technology and Advanced Engineering 2012; 2: 360-363.

[30] Shahbeig S. Retinal image analysis using multi-directional functors based on geodesic conversions. Turk J Electr Eng Co 2014; 22: 768-779.

[31] Shajahan SN, Roy RC. An improved retinal blood vessel segmentation algorithm based on multistructure elements morphology. International Journal of Computer Applications 2012; 57: 31-36.

[32] Yin Y, Adel M, Bourennane S. An automatic tracking method for retinal vascular tree extraction. In: IEEE International Conference on Acoustics, Speech and Signal Processing; 25–30 March 2012; Kyoto, Japan. New York, NY, USA: IEEE. pp. 709-712.

[33] Oliveira WS, Ren TI, Cavalcanti GDC. An unsupervised segmentation method for retinal vessel using combined filters. In: International Conference on Tools with Artificial Intelligence; 7–9 November 2012; Athens, Greece. New York, NY, USA: IEEE. pp. 750-756.

[34] Oliveira WS, Ren TI, Cavalcanti GDC. Retinal vessel segmentation using average of synthetic exact filters and hessian matrix. In: International Conference on Image Processing; 30 September–3 October 2012; Orlando, FL, USA. New York, NY, USA: IEEE. pp. 2017-2020.

[35] Johnson RC, Padmagireesan SJ, Raheem A, Pillai AV. Comparison of curvelet and contourlet transforms for retinal analysis. In: IEEE India Conference; 7–9 December 2012; Kochi, India. New York, NY, USA: IEEE. pp. 1214-1217.

[36] Silvia MJ, Poovizhi S. Retinal image analysis using ripplet-I transform and segmentation using morphological gradient. International Journal of Emerging Technology and Advanced Engineering 2012; 2: 719-724.

[37] Shanmugam V, Banu RSDW. Retinal blood vessel segmentation using an extreme learning machine approach. In: IEEE Point-of-Care Healthcare Technologies; 16–18 January 2013; Bangalore, India. New York, NY, USA: IEEE. pp. 318-321.

[38] Fraz MM, Remagnino P, Hoppe A, Barma SA. Retinal image analysis aimed at extraction of vascular structure using linear discriminant classifier. In: International Conference on Computer Medical Applications; 20–22 January 2013; Sousse, Tunis. New York, NY, USA: IEEE. pp. 1-6.

[39] Ocbagabir H, Hameed I, Abdulmalik S, Barkana Buket D. A novel vessel segmentation algorithm in color images of the retina. In: Applications and Technology Conference; 3 May 2013; Farmingdale, NY, USA. New York, NY, USA: IEEE. pp. 1-6.

[40] Asad AH, Azar AT, Fouad MMM, Hassanien AE. An improved ant colony system for retinal blood vessel segmentation. In: Federated Conference on Computer Science and Information Systems; 8–11 September 2013; Krakow, Poland. New York, NY, USA: IEEE. pp. 199-205.

[41] Sheet D, Karri SPK, Conjeti S, Ghosh S, Chatterjee J, Ray AK. Detection of retinal vessels in fundus images through transfer learning of tissue specific photon interaction statistical physics. In: International Symposium on Biomedical Imaging; 7–11 April 2013; San Francisco, CA, USA. New York, NY, USA: IEEE. pp. 1452-1456.

[42] Ceylan M, Yaşar H. Blood vessel extraction from retinal images using complex wavelet transform and complex-valued artificial neural network. In: International Conference on Telecommunications and Signal Processing; 2–4 July 2013; Rome, Italy. New York, NY, USA: IEEE. pp. 822-825.

[43] Candes EJ, Donoho DL. Curvelets-A surprisingly effective nonadaptive representation for objects with edges. In: Cohen A, Rabut C, Schumaker L, editors. Curves and Surface Fitting. Nashville, TN, USA: Vanderbilt University Press, 1999. pp. 105-120.

[44] Donoho DL, Duncan MR. Digital curvelet transform: strategy, implementation and experiments. In: SPIE on Wavelet Application VII; 5 April 2000; Orlando, FL, USA. Orlando, FL, USA: SPIE. pp. 12-30.

[45] Candes EJ, Guo F. New multiscale transforms, minimum total variation synthesis: application to edge-preserving image reconstruction. Signal Process 2002; 82: 1519-1543.

[46] Candes EJ, Donoho DL. New tight frames of curvelets and optimal representations of objects with piecewise-C^2 singularities. Commun Pur Appl Math 1999; 57: 219-266.

[47] Candes EJ, Demanet L, Donoho DL, Ying L. Fast Discrete Curvelet Transforms. Technical Report 2005. Pasadena, CA, USA: Applied and Computational Mathematics-California Institute of Technology.

[48] Neelamani R, Baumstein A, Ross W. Adaptive subtraction using complex-valued curvelet transform. Geophysics 2010; 75: V51-V60.

[49] He Y, Xing-Lan Z , Wei-Wei L, Feng C. Image restoration using Gaussian scale mixtures in complex curvelet transform domain. In: International Conference on Measuring Technology and Mechatronics Automation; 13–14 March 2010; Changsha City, China. New York, NY, USA: IEEE. pp. 427-430.

[50] Xu J, Yang L, Wu D. Ripplet: A new transform for image processing. J Vis Commun Image R 2010; 21: 627-639.

[51] www.curvelet.org (accessed 21 August 2014).

[52] Ceylan R, Ceylan M, Özbay Y, Kara S. Fuzzy clustering complex-valued neural network to diagnose cirrhosis disease. Expert Syst Appl 2011; 38: 9744-9751.